

Facing the Issues of Sheet Metal Equal-Channel Angular Pressing: A Modified Approach Using Stacks to Produce Ultrafine-Grained High Ductility AA5083 Sheets

Christian Illgen,* Benjamin Bohne, Martin F.-X. Wagner, Maximilian Gruber, Wolfram Volk, and Philipp Frint

A new approach for equal-channel angular pressing (ECAP) of thin AA5083 sheets using two different orientations is investigated to address the issues of sheet metal ECAP. The method includes the deformation of a stack of 6 individual sheets supported by bulk material pieces placed on both sides of the stack. An excess length of the support materials and their pre-deformation during an early stage of processing allows a buckling-free deformation of the thin sheets for one of the investigated orientations. Multiple ECAP passes (up to $N = 4$) at room temperature following route C and microstructural analyses by electron backscatter diffraction are performed. Two passes of ECAP already result in considerable grain refinement with equiaxed grains, pronounced substructures and in an increased tensile strength at room temperature. At elevated temperatures (250 °C) a comparatively large elongation to failure ($> 130\%$) is found for the fine-grained sheets. Diffusion-controlled deformation mechanisms likely contribute to the deformation behavior of the investigated material. Scanning electron microscopy of the tensile specimens after testing reveals the formation of elongated and large cavities. These results highlight the suitability of the modified experimental method to produce (ultra)fine-grained thin aluminum sheets with distinctly increased strength and ductility.

technological^[2] point of view. As ECAP was originally intended for processing of bulk materials,^[3] ECAP dies typically exhibit channels with rectangular or circular cross sections. In the past four decades, a lot of effort has been put into the development of variations and enhancements of the ECAP process. These developments are basically twofold: on the one hand, technologically oriented research is aiming for upscaling^[4,5] and commercialization;^[6,7] on the other hand, fundamental materials science endeavors to improve the understanding of the relationship between microstructural evolution and large plastic strains.^[1] Many studies have dealt with the influence of factors related to processing on the microstructural evolution of different materials, e.g., pressing speed,^[8] temperature,^[9] back pressure,^[10] lubrication,^[11,12] or processing routes.^[13,14] While the influence of such process parameters has been extensively studied since the introduction of ECAP, there has only been major research activity with a focus on the work

1. Introduction


Equal-channel angular pressing (ECAP) is an attractive method for grain refinement from a scientific^[1] and from a

piece geometry^[15] during the past decade. Especially the processing of work pieces with a large aspect ratio, like sheets and plates, has recently gained increasing interest. A particularly attractive feature of ultrafine-grained (UFG) sheet materials is, for instance, their ability to undergo large strains at elevated temperatures and low strain rates, even up to superplastic behavior.

Two approaches for ECAP of sheet materials can be distinguished: either adapting the channel geometry to the dimensions of the work piece (single sheet approach) or adapting the work piece to a given channel geometry by stacking a corresponding number of sheets (stacked sheets approach, see also **Figure 1**). The single sheet approach has been reported to work quite well for relatively thick sheets and plates (thickness e.g., ≈ 5 mm).^[15] Thin sheets (≈ 2 – 3 mm or below) have also been equal-channel angular (ECA)-processed with this approach.^[16,17] Suh et al.^[18] have demonstrated that grain refinement, texture changes (which are also observed during bulk ECAP^[19]) and improved drawability in subsequent forming operations can be achieved by deforming magnesium sheets at elevated temperatures in a custom built, laterally opened single sheet ECAP die. However, pushing the sheet into the die's shear zone (which is typically fan

C. Illgen, B. Bohne, Prof. M. F.-X. Wagner, Dr. P. Frint
Institute of Materials Science and Engineering
Technische Universität Chemnitz
Erfenschlager Str. 73, Chemnitz D-09125, Germany
E-mail: christian.illgen@mb.tu-chemnitz.de

M. Gruber, Prof. W. Volk
Chair of Metal Forming and Casting
Technische Universität München
Walther-Meißner-Str. 4, Garching D-85748, Germany

 The ORCID identification number(s) for the author(s) of this article can be found under <https://doi.org/10.1002/adem.202100244>.

© 2021 The Authors. Advanced Engineering Materials published by Wiley-VCH GmbH. This is an open access article under the terms of the Creative Commons Attribution License, which permits use, distribution and reproduction in any medium, provided the original work is properly cited.

DOI: 10.1002/adem.202100244

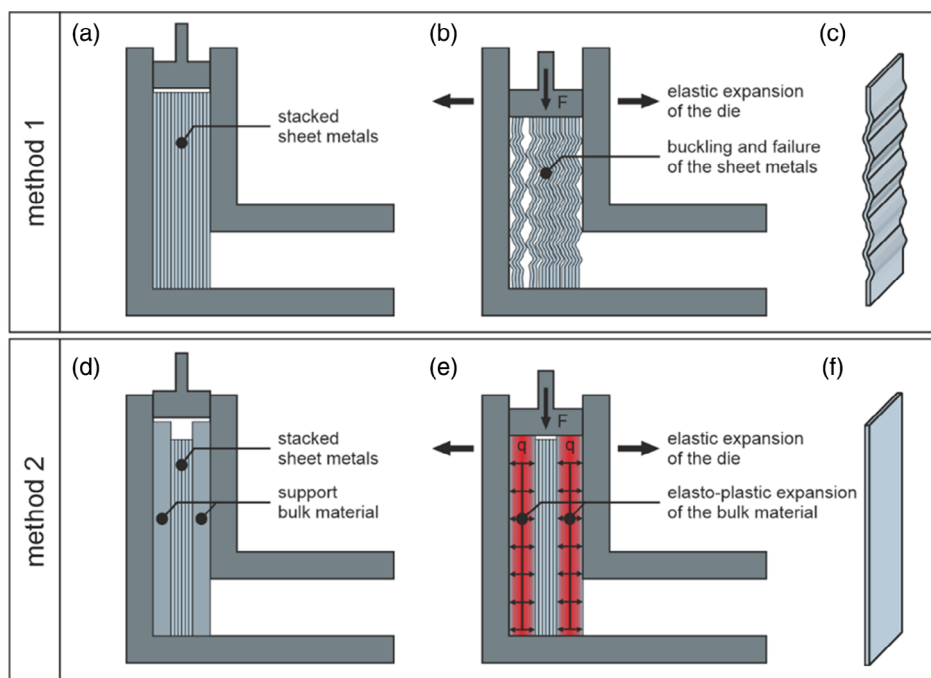


Figure 1. Two methods for ECAP processing of sheet metals (schematic): a) method 1 uses stacked sheet metals to completely fill the entrance channel. b) However, elastic expansion of the ECAP die under loading may result in buckling and failure of individual sheets during processing; c) buckled sheet. d) Method 2 instead uses stacked sheet metals supported by two bulk material pieces with excess length. e) The elastic expansion of the ECAP die under loading is compensated by the elasto-plastic expansion of the compressed bulk materials, resulting in some quasi-hydrostatic pressure, q ; f) plain, damage-free sheet.

shaped^[20]) using a conventional plunger often tends to cause upsetting of the sheet and localization of shear deformation, resulting in a poor surface quality or even in material failure.^[21] In addition, through-thickness residual stresses associated with a pronounced bending deformation have been documented^[22] after single sheet ECAP. Such stresses may be particularly harmful during subsequent (superplastic) forming operations as they may lead to premature failure.

The stacked sheets approach in principle represents a promising alternative without these drawbacks because thin sheet materials can potentially be processed in conventional, well-developed ECAP dies.^[23,24] However, the results presented in the study by Lachhab et al.^[24] on processing a stack of 9 Fe–48 wt%Ni sheets also show that stacks may be prone to sliding between individual sheets, which further results in heterogeneous shear deformation with superimposed bending, in correspondingly heterogeneous grain sizes, mechanical properties, and textures that ultimately also depend on an individual sheet's position in the stack. Obviously, further improvements are needed to fully exploit the potential of the stacked sheets approach and to meet an essential requirement: providing a homogeneous and well-defined shear deformation throughout the stack of sheets.

One goal of this study is to address the issues associated with the stacked sheets approach. Multiple ECAP passes on AA5083 aluminum sheets are carried out, adding support materials adjacent to the stacked sheets, and with different stack orientations. It is shown that a novel stack orientation, resulting in in-plane shear deformation of individual sheets, leads to homogeneous

deformation of the entire stack. Moreover, first results from electron microscopy and differential scanning calorimetry (DSC) that indicate substantial grain refinement in the ECA-pressed sheets are presented. Finally, tensile testing at ambient and elevated temperatures demonstrates the sheets' suitability for subsequent forming operations.

2. Experimental Section

A large scale, friction reduced 90°-ECAP die with sliding walls was used for processing of cold-rolled AA5083 aluminum sheets (4.81 wt% Mg, 0.53 wt% Mn, 0.36 wt% Si, 0.23 wt% Fe, and 0.18 wt% Cr, bal. Al) with a thickness of 1.7 mm. The die, described in greater detail in the study by Frint et al.,^[4] fulfills the criteria for optimum ECAP processing as defined by Segal.^[2] For example, it allows for the application of a sufficient back pressure, which is a key requirement for the introduction of a homogeneous shear deformation in ECAP of bulk materials. Moreover, the die has a large channel cross section of 50 × 50 mm², which in the context of this study facilitates processing of multiple sheets using the stacked sheets approach described above. A fundamental challenge associated with this approach, however, is to prevent the sheets from buckling during processing while introducing a homogeneously distributed shear deformation into the material. Figure 1 schematically shows the principle of processing stacked sheets in an ECAP die with a square cross-section, highlighting two different methods that can be applied to completely fill the entrance channel. Method 1,

proposed by Lachhab et al.,^[24] is characterized by stacking the appropriate number of sheets (depending on the sheet thickness) needed to completely fill out the channel, see Figure 1a. However, as some clearance is needed for inserting a billet (or stack of sheets) into the channel, and because loading during processing leads to an elastic expansion of the die, some additional clearance is generated during the ECAP process and this results in buckling of the sheets, as shown in Figure 1b,c. To solve these issues, the novel method 2 (see Figure 1d) is introduced in this study. A smaller number of sheets is used to form the stack and additional bulk material pieces are placed on both sides of the stack to fill out the entrance channel of the die. The bulk material pieces protrude from the end of the stack near the surface of the plunger, which leads to elasto-plastic deformation during the onset of processing. This predeformation allows to compensate for both the initial clearance and the clearance created by the elastic expansion of the die. It furthermore produces a quasi-hydrostatic pressure (q) in the stack (see Figure 1e). This additional mechanical constraint is expected to have a positive effect on the shear deformation and to prevent material failure, which is often related to local tensile stresses during ECAP.^[25] The shear deformation, superimposed by a hydrostatic pressure, consequently allows the production of plain, damage-free sheets (see Figure 1f).

Figure 2 shows an overview of the setup of the stacks used in this study. Six individual sheets with a thickness of 1.7 mm, all oriented with the rolling direction (RD) parallel to the pressing direction of the ECAP die (see Figure 2a), and the supporting bulk material pieces were assembled, as shown in Figure 2b. The resulting stacks of sheets and bulk pieces (referred to as work pieces hereafter) were machined by milling to obtain a final cross section of slightly less than $50 \times 50 \text{ mm}^2$ (see Figure 2b) to facilitate stress-free insertion into the die's entrance channel. It is particularly important to note that, because of the square cross-section of the die, a work piece can in principle be inserted into the entrance channel with two different orientations, see Figure 2c,d. To the best of our knowledge, all previous studies on the stacked sheets approach used a stack orientation, as shown in Figure 2c, with an alignment of the normal direction

(ND) of the sheets parallel to the x -direction (i.e., the orientation of the ECAP die's exit channel), as shown in Figure 2c. This orientation is referred to as stack orientation A. Figure 2d shows that the second stack orientation, stack orientation B, is instead obtained by a 90° rotation of the work piece around its longitudinal axis, which corresponds to a parallel alignment of the sheets' NDs to the y -direction. It should be noted that for each individual component of the stack this deformation behavior is similar to that during ECAP in the "vertical configuration" as presented by Kamachi et al. for individual plates.^[26]

Considering the orientation of the plastic deformation zone (PDZ, with an opening angle Ψ and primary shear directions shown schematically in Figure 2c,d), it is obvious that stack orientation A primarily leads to shear strains in the ND–RD plane of the sheets, whereas stack orientation B results in shear deformation in the RD–transverse direction (TD) plane. While results from ECAP experiments using stack orientation A can be compared with previous studies, the in-plane shear deformation produced by ECAP with the novel stack orientation B can clearly be expected to provide unconventionally sheared sheet samples with potentially uncharted microstructure–property relationships. In this study, the effect of ECAP using both stack orientations (with a more pronounced focus on stack orientation B) is investigated.

Prior to ECAP, the work pieces consisting of the stacked sheets and the support materials were annealed at 500°C for 1 h to ensure an initial condition free of potential microstructural traces of previous strain hardening. To reduce friction during ECAP, the work pieces were coated with a lubricant (Bechem BERUFORGE 150 D).^[11] To achieve pronounced grain refinement and to avoid any effects of local heating, ECAP was carried out at room temperature and at a low pressing speed of 10 mm min^{-1} . A back pressure of 75 MPa was applied to reduce the size of the PDZ as characterized by a small opening angle. The equivalent plastic strain can then be estimated as about 1.1.^[20,27] One ECAP pass ($N = 1$) was carried out on both stack orientations, and multiple passes ($N = 2, 4$) could additionally be investigated in the case of stack orientation B. During the first pass of ECAP, the (as-received) RD of the sheets was always parallel to the extrusion direction. For processing by multiple

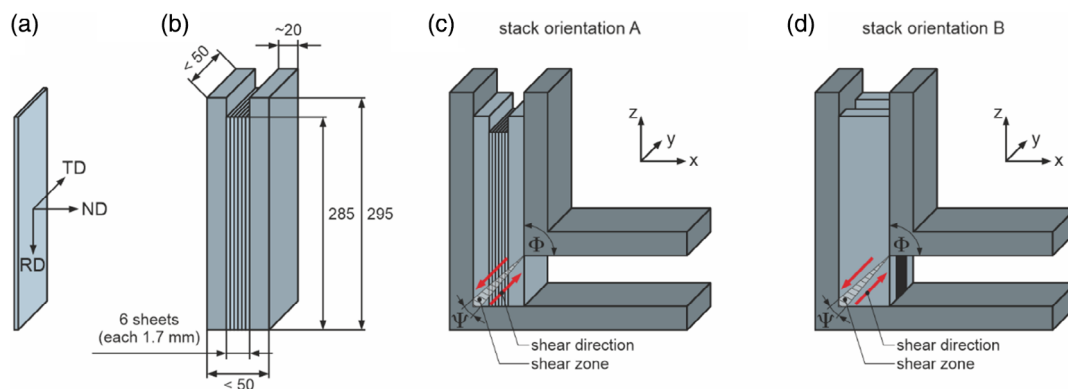


Figure 2. a) Single sheet with relative orientations of RD, ND, and TD, respectively, as used in this study. b) Dimensions of a work piece consisting of six stacked sheets, supported by two bulk material pieces. Two stack orientations can be used to perform ECAP on a stacked work piece: c) stack orientation A leads to shear deformation in the ND–RD plane of the sheets, whereas d) the novel stack orientation B is associated with shearing in the RD–TD plane.

ECAP passes ($N = 2, 4$) route C was applied. This route corresponds to a 180° rotation of the work pieces around their longitudinal axes between individual passes. It was shown to effectively promote the formation of fine, globular grains, which is an important prerequisite for superplastic behavior in sheet materials. Prior to each additional ECAP pass ($N > 1$), the deformed work pieces were annealed for 1 h at a temperature of 180°C to maintain a sufficient potential for further work hardening without premature failure of the material. The support pieces were machined to exhibit some additional excess length prior to each additional ECAP pass.

To characterize the thermal stability of the deformed sheet samples, and to determine an optimum temperature for tensile testing, DSC was carried out with a heating rate of 20 K min^{-1} in the temperature range from room temperature to 500°C using a Mettler Toledo DSC1 device. The DSC tests took place in a furnace chamber with nitrogen inert atmosphere and with Al 5N high-purity aluminum (Al99,999%) as a reference material. All measurements were carried out with three repeating cycles of the same temperature profile.

Tensile specimens with a gauge length of 19 mm and a width of 4 mm were taken by means of wire electrodischarge machining parallel to the extrusion direction of the sheets. Mechanical characterization was carried out by quasi-static ($\dot{\epsilon} = 10^{-3}\text{ s}^{-1}$) uniaxial tensile testing in a Zwick/Roell 100 kN tensile testing machine equipped with a standard load cell. To study the relationship between microstructural changes associated with ECAP and temperature-dependent mechanical behavior, tensile tests at room temperature and at elevated temperatures (250°C) were carried out on specimens obtained after different numbers of ECAP passes ($N = 1, 2, \text{ and } 4$). In case of room temperature testing, sample elongation was recorded using digital image correlation (DIC). Tensile testing at elevated temperatures was carried out in a custom-built tube furnace that allows for relatively high pretest heating rates (a stable testing temperature of 250°C was reached after 23 min, compared with 85 min needed in a conventional furnace) and precise temperature control, which is of particular importance when testing UFG materials. During testing at elevated temperatures, crosshead-displacement data were used to determine tensile strains.

Samples for microstructural investigations were subjected to a conventional mechanical grinding and polishing procedure followed by colloidal silica polishing. The microstructural features of initial and deformed material conditions were examined in the RD–TD (x – z) plane of the sheets. For scanning electron microscopy (SEM) as well as electron back-scatter diffraction (EBSD), a Zeiss Neon 40 EsB field-emission scanning electron microscope equipped with a DigiView IV EBSD camera (EDAX Inc., Mahwah, NJ, USA) was used with an acceleration voltage of 15 kV and a step size of 200 nm. EBSD raw data were postprocessed by a slight clean-up including a confidence index-neighbor correlation and grain dilation. Grains in the OIM analysis software (ver. 6) were defined as having a minimum grain size of 3. Grain tolerance angles of 5° (TA- 5°) and 15° (TA- 15°) were used for characterization of substructures and grains with high-angle grain boundaries (HAGBs), respectively. In addition, energy dispersive X-ray spectroscopy (EDX) was carried out in the SEM to analyze chemical composition.

3. Results and Discussion

3.1. Initial Microstructure

Figure 3 shows the initial microstructure of the annealed AA5083 sheets observed in the RD–TD plane by EBSD. Dark spots (highlighted by white arrows) in the image quality map (IQ) shown in Figure 3a indicate primary precipitates. The accompanying EDX measurements (results not shown here) indicate that these precipitates contain iron and manganese, which is typically observed for Al₆(Mn, Fe) precipitates. The orientation map (OM) in Figure 3b shows a microstructure of homogeneously distributed, equiaxed grains. Black lines represent HAGBs with misorientations larger than 15° . For a grain tolerance angle of 5° , a mean grain size of $42\ \mu\text{m}$ can be observed, while the mean grain size for a tolerance angle of 15° is significantly higher ($GS_{\text{TA-}15^\circ}$: $87\ \mu\text{m}$). This agrees well with the relatively broad peaks in the grain size distribution (plotted as area fraction vs grains size in Figure 3c) between 25 and $95\ \mu\text{m}$ (TA- 5°) and 35 and $185\ \mu\text{m}$ (TA- 15°), respectively. The pole figures in Figure 3d, determined from the EBSD data and thus representative of local microtexture, are in line with the rolling texture typically expected for previously cold-rolled aluminum sheets.^[28]

3.2. Effect of Stack Orientation on Macroscale Homogeneity of Deformation

The feasibility of using the two stack orientations was examined and evaluated by considering the macroscale deformation of the stacked work pieces after the first pass of ECAP, Figure 4. Obviously, in case of stack orientation A, the deformed work piece exhibits substantial failure and heterogeneous deformation of the individual sheets as well as of the support materials, especially at the front and rear ends of the stack (see Figure 4a). Regardless of the application of back pressure, low pressing speeds, and good lubrication, the deformation of the work piece clearly indicates that a fan-shaped PDZ, associated with a minor strain gradient, was formed during ECAP, as described in detail in the studies by Wagner and coworkers.^[20,29] While in conventional billets that consist of a bulk material, minor local strain differences can be compensated in the microstructure (although more pronounced strain gradients lead to distinct heterogeneities or even to partitioning in the resulting microstructural features and mechanical properties^[25]), a work piece that consists of several stacked sheets involving many interfaces is particularly prone to sliding between sheets as discussed above. Of course, a similar strain gradient related to the formation of a nonvanishing PDZ also occurs when processing a work piece in stack orientation B. However, the essential difference is that this gradient is identical in magnitude and direction for each individual component of the stack (support material or sheet). Therefore, no relative motion between individual sheets or between sheets and support material occurs in stack orientation B, and the ECAP-deformed sheets do not show buckling or failure but instead remain plane, Figure 4b. These observations shown in Figure 4 clearly

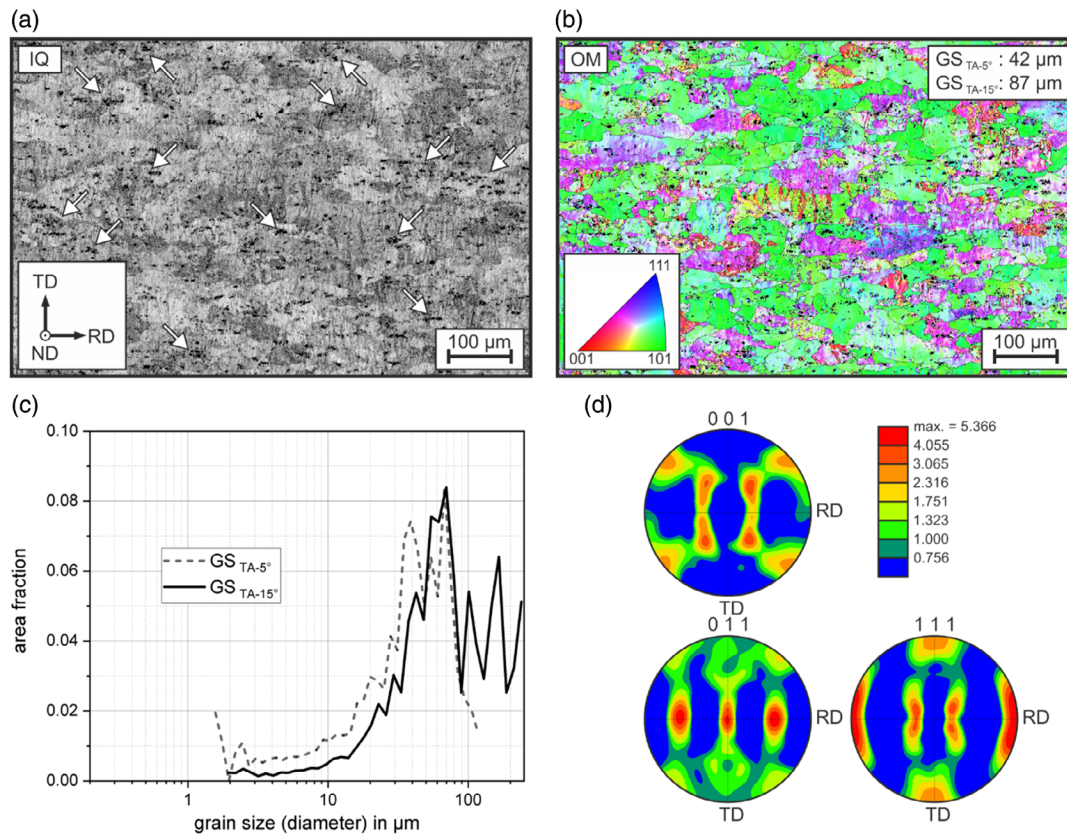


Figure 3. Initial microstructure of the investigated AA5083 sheet material analyzed by EBSD: a) White arrows in the IQ highlight primary Al₆(Mn, Fe)-type precipitates. b) The OM shows a homogeneous microstructure with equiaxed grains. c) Grain size distributions for grain tolerance angles of 5° and 15°. d) Pole figures calculated from the EBSD data indicate a typical rolling texture.

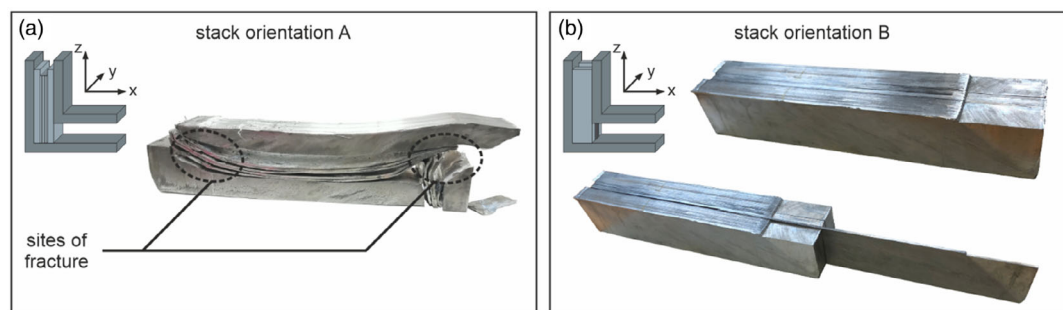


Figure 4. ECAP work pieces after processing with different stack orientations: a) ECAP with stack orientation A is associated with pronounced sliding between sheets, and with failure near both ends of the work piece. b) In contrast, ECAP with stack orientation B allows to produce plane sheets in single or even in multiple ECAP passes.

demonstrate that only stack orientation B can be used to carry out multiple passes of ECAP on the AA5083 sheets investigated in this study. Therefore, in the remainder of this article, investigations are focused on microstructural changes, thermal stability, and mechanical properties of ECA-processed sheets using stack orientation B.

3.3. Microstructural Changes during Multiple-Pass ECAP Using Stack Orientation B

Figure 5 shows representative EBSD micrographs of the ECAP-processed material in the N1, C2, and C4 conditions (i.e., after 1, 2, and 4 passes using route C) accompanied by the corresponding

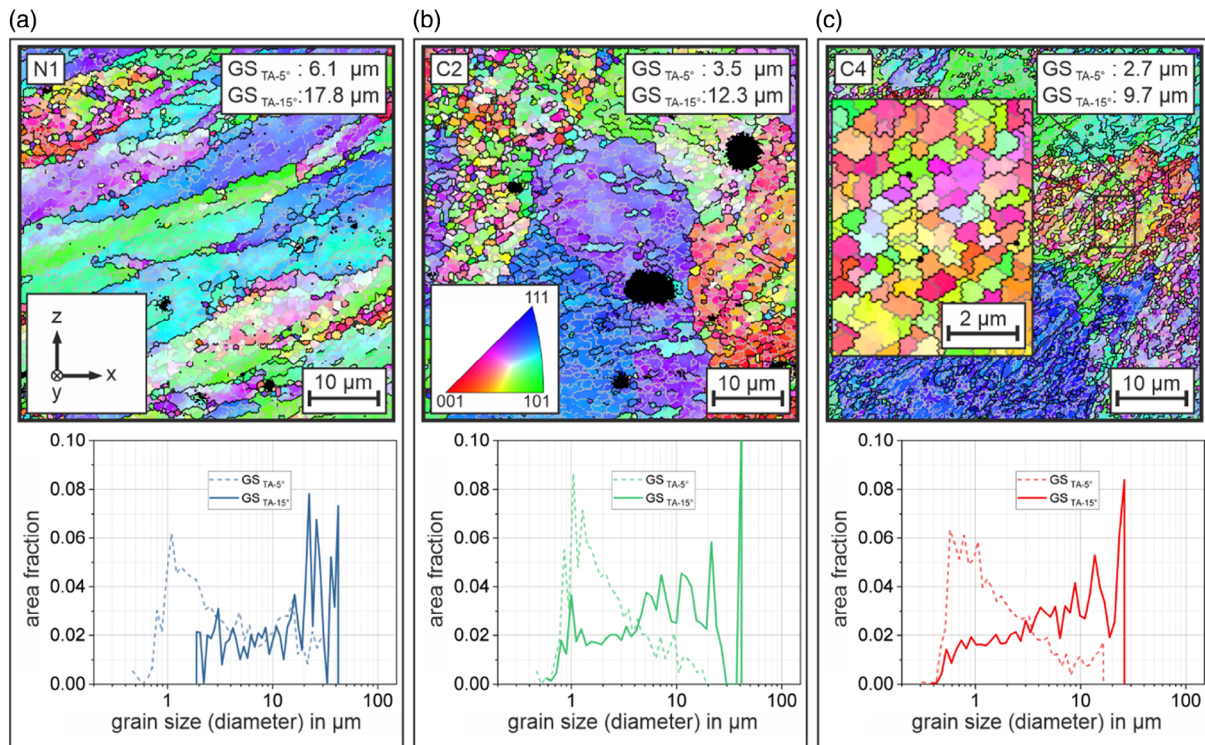


Figure 5. Microstructures after ECAP with stack orientation B and different numbers of passes. OMs and corresponding grain size distributions GS_{TA-15° and GS_{TA-5° of the sheet metals after a) a single pass of ECAP (N1), b) two accumulative ECAP passes (C2), and c) four passes of ECAP (C4) using route C.

grain size distributions. To characterize both deformation-induced substructures with relatively low misorientations and grains with HAGBs, grains were defined by two different grain tolerance angles (5° and 15°). Each micrograph represents the x - z plane as defined in the die-related coordinate system (see Figure 2). Black lines again represent HAGBs with misorientations larger than 15° , whereas additional gray lines correspond to boundaries with misorientation angles between 5° and 15° . Some dark spots correspond to primary precipitates which were excluded from the EBSD indexing procedure. Figure 5a shows the microstructure after a single pass of ECAP (N1), which is characterized by highly elongated grains and pronounced heterogeneities; areas with large deformation and distinct grain refinement are located next to areas with much lower deformation. The longitudinal semiaxes of the elongated grains are oriented at a certain characteristic tilt angle with respect to the x direction. This tilt angle typically varies between $\approx 23^\circ$ and 26° for a 90° -ECAP die, depending on the opening angle of the fan-shaped PDZ.^[30] This agrees well with the tilt angles shown in Figure 5a. The corresponding grain size distribution (TA- 15°) has characteristics of a bimodal microstructure, with a relatively wide spread between about 2 and 42 μm . After the first pass of ECAP, the average grain size is already reduced to about $GS_{TA-15^\circ} = 17.8 \mu\text{m}$ and $GS_{TA-5^\circ} = 6.1 \mu\text{m}$, respectively.

The EBSD micrograph of the material deformed in two accumulative ECAP passes (C2) in Figure 5b shows a more homogeneous microstructure with an average grain size of $GS_{TA-15^\circ} = 12.3 \mu\text{m}$ ($GS_{TA-5^\circ} = 3.5 \mu\text{m}$). Former elongated grains are almost equiaxed again, which is expected for even numbers

of passes following route C.^[13] They contain pronounced substructures (grey lines) that are characterized by distinctly large misorientations ($> 5^\circ$). In contrast to the bimodal microstructure of the N1 material, the grain size distribution (TA- 15°) for C2 reveals that a considerable fraction of the grains already has a diameter of about 1 μm . This indicates an early stage of grain refinement. After two further ECAP passes (C4), an even more refined microstructure with equiaxed grains and a mean grain size of $GS_{TA-15^\circ} = 9.7 \mu\text{m}$ ($GS_{TA-5^\circ} = 2.7 \mu\text{m}$) is observed (Figure 5c). The grain size distribution (TA- 15°) is shifted to smaller grain sizes, whereas the shape of the grain size distribution function remains almost unchanged compared with C2, which is characteristic for this number of ECAP passes. As often reported in the literature for bulk materials, the microstructural changes become less pronounced with an increasing number of accumulative ECAP passes. Based on the microstructural results discussed here (Figure 5), the same conclusion can be drawn for the processing of sheet materials. This also highlights the potential of sheet metal ECAP for grain refinement when using the stacked sheets approach and stack orientation B.

It should be mentioned that even the condition up to four accumulative ECAP passes (C4) represents a precursor to UFG microstructures. Consequently, all ECAP-deformed microstructures may still be dominated by a high amount of low-angle grain boundaries (LAGBs) or by a transition from LAGBs to HAGBs. To address the stage of grain refinement, Figure 6a shows the boundary line length per area (boundary density) as a function of the misorientation angle accompanied by Figure 6b the number fraction and cumulative distribution

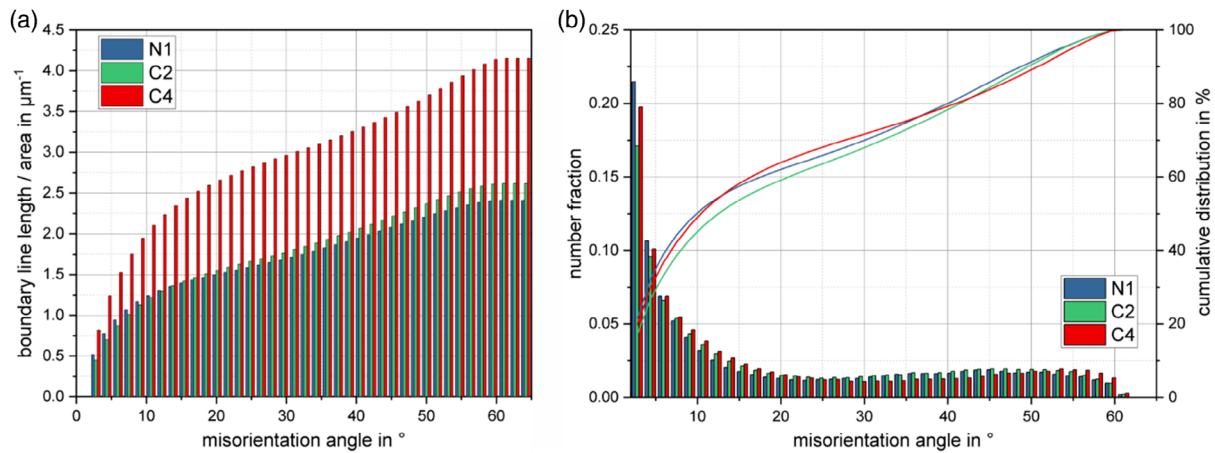


Figure 6. Quantitative analysis of the boundary characteristics of the severely deformed sheet metal. a) Boundary density as a function of the misorientation angle, b) number fraction and cumulative distribution of the boundaries as a function of the misorientation angle.

function of the corresponding misorientation angles. The misorientation distributions of all ECAP conditions are similar. Only minor differences can be observed at large misorientations ($> 50^\circ$) where the C4 condition shows increased fractions compared with N1 and C2. This impression is also confirmed by the corresponding cumulative distribution functions. The similarity of the misorientation distributions is most likely related to the processing of the material. As a recovery heat treatment was carried out prior to each subsequent ECAP pass, it is assumed that the defect density is considerably reduced due to annihilation processes. This results in an increased strain hardening capacity in the following ECAP pass and consequently in the reformation of defect structures with LAGBs.

For a further quantification of the stage of grain refinement, the boundary density distributions are shown in Figure 6a. A comparison of the N1 and the C2 conditions reveals a slight increase in the boundary density for large misorientation angles ($> 15^\circ$) that is accompanied by a decrease for low misorientations ($< 15^\circ$). This result shows a transition from LAGBs to HAGBs caused by SPD processing. This is even more pronounced for the C4 condition, which shows a considerably increased density for all misorientation angles, especially for misorientations larger than 15° . It can be concluded that even the microstructures after multiple ECAP passes are dominated by low-angle boundaries. In combination with the micrographs and grain size distributions shown in Figure 5, this observation underlines that all investigated conditions are still precursors to a fully UFG microstructure. However, the mean grain size for both definitions (substructures and HAGBs) is already reduced by $\approx 90\%$ after 4 ECAP passes compared with the initial condition.

3.4. Thermal Analysis

Materials processed by SPD often exhibit a low thermal stability because they are usually characterized by a high density of lattice defects, and therefore prone to early recovery and pronounced recrystallization. Additional thermally activated processes like grain boundary sliding are also particularly relevant when one considers superplastic behavior of UFG materials. In the context

of this study, it is therefore important to characterize the mechanical behavior at elevated temperatures while also considering the predominant microstructural changes that affect thermal stability in the corresponding temperature range.

Figure 7 shows the results of a DSC measurement for the initial material condition as well as for the material deformed in four accumulative ECAP passes (C4). The initial condition (gray curve) of the non-age hardening aluminum alloy shows no endothermic or exothermic reactions in the examined temperature range, which demonstrates the thermal stability of its microstructure. In contrast, after four ECAP passes (C4) the DSC curve shows distinct exothermic (exo) peaks. In the temperature range from 100 to 225°C , a comparatively broad exothermic peak can be observed. It most likely results from recovery of the work-hardened microstructure. A second, more pronounced exothermic process starts at about 290°C and reaches its peak at $\approx 310^\circ\text{C}$. The well-defined DSC peak can be attributed to recrystallization of the fine-grained microstructure, which is completed

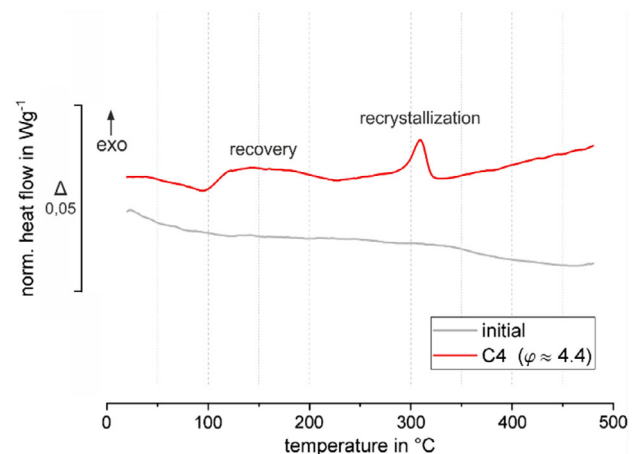


Figure 7. DSC heat flow curves for AA5083 sheet metals in initial and ECAP-deformed material conditions (C4). Thermally induced recovery starts at $\approx 100^\circ\text{C}$ and a pronounced recrystallization peak is observed at about 310°C .

at about 320 °C. The subsequent steady increase in the heat flow is most likely related to grain growth at higher temperatures. Considering superplastic deformation of the processed sheet materials, processing temperatures need, on the one hand, to be increased as far as possible to promote diffusion-controlled microstructural mechanisms; on the other hand, the onset of dynamic recrystallization and grain growth enforce an upper limit on the useful temperature range. From the DSC data, an ideal processing temperature of 250 °C was identified and used in subsequent tensile tests at elevated temperatures.

3.5. Mechanical Behavior at Room Temperature

Figure 8 shows the results of the quasi-static tensile tests at room temperature for the initial and for three ECAP-deformed material conditions (N1, C2, and C4), represented by engineering stress–strain curves in Figure 8a. Both the initial and the ECAP-deformed aluminum sheet materials exhibit a typical serrated flow in all conditions due to the Portévin–Le Châtelier (PLC) effect.^[31–33] The increase in yield strength (YS) as well as the decrease in elongation to failure (EF) are shown in Figure 8b,c as a function of the performed accumulative ECAP passes. The initial condition (gray curve in Figure 8a) shows a YS of 130 MPa and an EF of ≈21%. After a single pass of ECAP (N1), a strong increase in the YS to 389 MPa can be observed, which corresponds to an increase of 200% compared with the initial condition. At the same time, the EF decreases to a value of 7%. Both effects can be attributed to a pronounced increase in the defect density due to work hardening and to the beginning formation of substructures. The increase/decrease in the strength/ductility is less pronounced during subsequent ECAP passes (C2, C4). Only a minor increase in YS to 423 MPa (increase of only an additional 9%) and a decrease in EF to 5.2% is observed for C2. This might be attributed to the formation of more pronounced substructures with enlarged misorientation angles in comparison to N1 (see also Figure 5). Two additional ECAP passes (C4) result in only minor changes of the

mechanical properties (YS 448 MPa, EF 5.1%). With an increasing number of ECAP passes the material shows less pronounced work hardening. Especially, the fine-grained material (C4) already reaches its ultimate tensile strength at an elongation of ≈2%. It is well known that (ultra)fine grains only provide a small mean free path for dislocation motion, which results in a low ductility related to dislocation slip at room temperature. The results of the microstructural analyses and the room temperature tensile tests confirm that the representative characteristics that have previously been reported for bulk materials are also observed after sheet metal ECAP when using stack orientation B.

3.6. Mechanical Behavior at 250 °C

As severely deformed materials often exhibit a low thermal stability and UFG microstructures are susceptible to changes in the (thermally activated) deformation mechanisms, a significantly different mechanical behavior is found at elevated temperatures. Figure 9 shows the results of the quasi-static tensile tests at 250 °C for the investigated material conditions (initial, N1, C2, and C4). In contrast to the increase in strength with increasing number of ECAP passes at room temperature, a distinct decrease in strength is observed in the engineering stress–strain curves in Figure 9a. The initial material condition (gray curve) shows a YS of 107 MPa and an EF of ≈65%. The strength is reduced by 47% after a single pass of ECAP. Further ECAP passes lead to additional, minor reductions in strength, as shown in Figure 9b.

For a discussion of strain-hardening behavior, true stress–strain curves are additionally shown in Figure 9a. This allows to distinguish better between material and specimen geometry related softening. The calculation of true stress–strain curves from the engineering curves is only strictly valid prior to the onset of necking (marked by small circles). During unstable plastic deformation, true stress and strain values are only estimated and therefore these parts of the curves are plotted as dashed lines. Figure 9a shows a pronounced softening in the engineering stress–strain curves, which is characterized by an almost

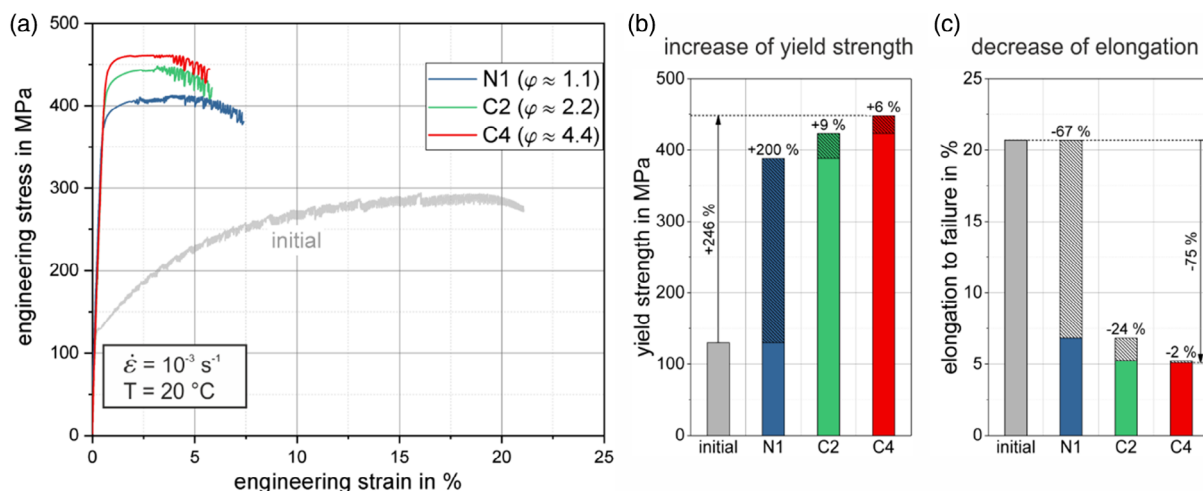


Figure 8. a) Engineering stress–strain curves from tensile testing of the initial (gray) and ECAP-processed (N1 blue, C2 green, and C4 red) sheet metals at room temperature under quasi-static loading conditions; b) increase in YS, and c) decrease in EF as a function of the number of ECAP passes using stack orientation B.

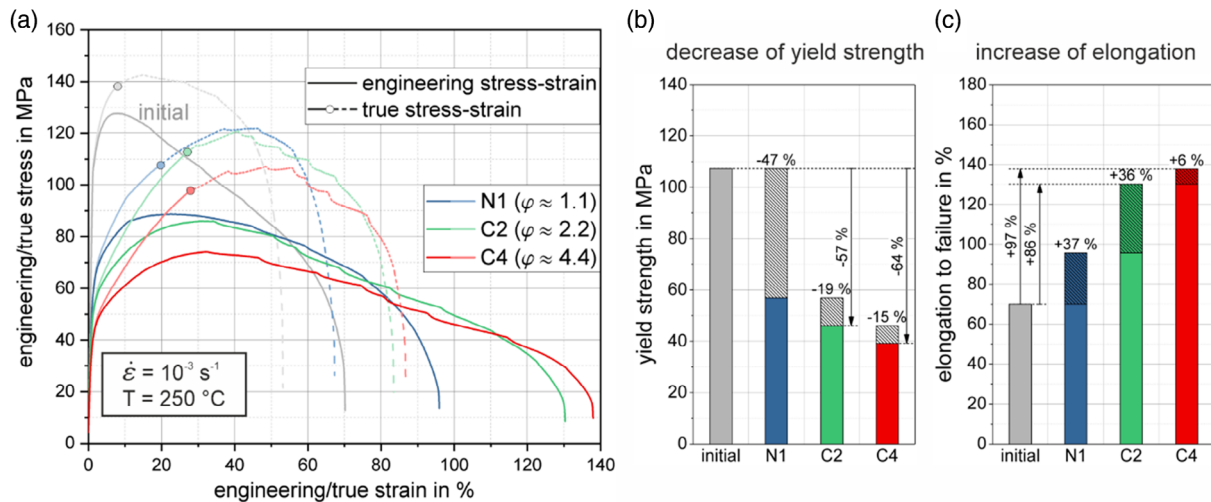


Figure 9. a) Engineering/true stress–strain curves from tensile testing of the initial (gray) and ECAP-processed (N1 blue, C2 green, and C4 red) sheet metals at 250 °C under quasi-static loading. For the true stress–strain curves, the onsets of instability are marked by small circles and the further nonuniform elongation is plotted by dashed lines. b) Decrease in YS, and c) increase in EF (engineering stress/ strain).

linear decline of the stress–strain curve after the onset of necking. The further increasing stresses in the true stress–strain curves after the onset of instability and a distinct strain hardening capacity indicate that most of the apparent strain softening in the engineering stress–strain curves is in fact simply geometrical. In contrast to the typical characteristics of a progressive localization of strain during tensile testing (of coarse-grained materials at room temperature), the ECAP materials show a wide necking area extended to a relatively large fraction of the gauge length (see also **Figure 10**). This large necking area and its continuous deformation during tensile straining result in the almost linear decline of the engineering stress–strain curves. This deformation behavior in terms of necking is an often-observed phenomenon for superplastic materials.^[34] For all material conditions the softening-related (nonuniform) elongation is larger than the uniform elongation that occurs during strain hardening. The ratio of elongation to failure to uniform elongation in all engineering stress–strain curves is about 10 for the initial material condition, whereas it is ≈ 4 for all ECAP-deformed material conditions. The waviness of the curves during strain softening, mainly noticeable in condition C2 and C4, is likely related to a weak PLC effect. Furthermore, the negative slopes of the engineering curves related to geometrical softening decrease with increasing number of ECAP passes (N1, C2, and C4).

Compared with the deformation behavior at room temperature (Figure 8), the results shown in Figure 9b,c indicate the presence of a different deformation behavior at 250 °C, which is controlled by pronounced recovery and most likely by a contribution of additional diffusion-controlled deformation mechanisms. Despite of the increased defect density after a single pass of ECAP (N1), which results in an increased density of obstacles for dislocation motion, a distinctly reduced strength is found compared with the initial material condition. This is a further indication that deformation mechanisms other than conventional dislocation slip may also contribute to the deformation behavior at 250 °C. According to Hsiao and Huang,^[35] three

different, diffusion-controlled deformation mechanisms can contribute to the deformation behavior of SPD-processed AA5083: power-law dislocation creep, solute drag creep, and grain boundary sliding. The relative contributions of these processes depend on the microstructure (degree of grain refinement, defect density) and on temperature. Grain boundary sliding in particular takes place in microstructures characterized by large misorientations and small equiaxed grains. As shown in Figure 6, the fraction of HAGBs increases with the number of ECAP passes (N1, C2, and C4) and especially for C4 small equiaxed grains can be observed (see inset in Figure 5c). However, as noted earlier, the ECAP-deformed conditions in this study still represent precursors to fully developed UFG-microstructures, and they are dominated by a large number of LAGBs and substructures. It is therefore likely that a gradual change in the predominant deformation mechanisms toward several diffusion-controlled processes occurs. It should be pointed out that compared with the initial condition almost a doubling of the elongation (in terms of engineering strains) is observed for the materials deformed by multiple ECAP passes (C2, C4), which underlines the potential of the used approach to create UFG sheet materials.

3.7. Cavity Formation during Tensile Testing at Elevated Temperatures

Plastic deformation at elevated temperatures typically leads to the formation of characteristic cavities in the microstructure. These cavities, which are commonly observed in conventional superplastic materials,^[36] are associated with diffusion-controlled deformation mechanisms and interface-related phenomena at primary precipitates.^[37] In some cases, the formation of cavities has also been related to small vacancy clusters developing during SPD.^[38,39] **Figure 10** shows SEM micrographs (back-scattered electron contrast) of the initial, N1, C2, C4 material conditions,

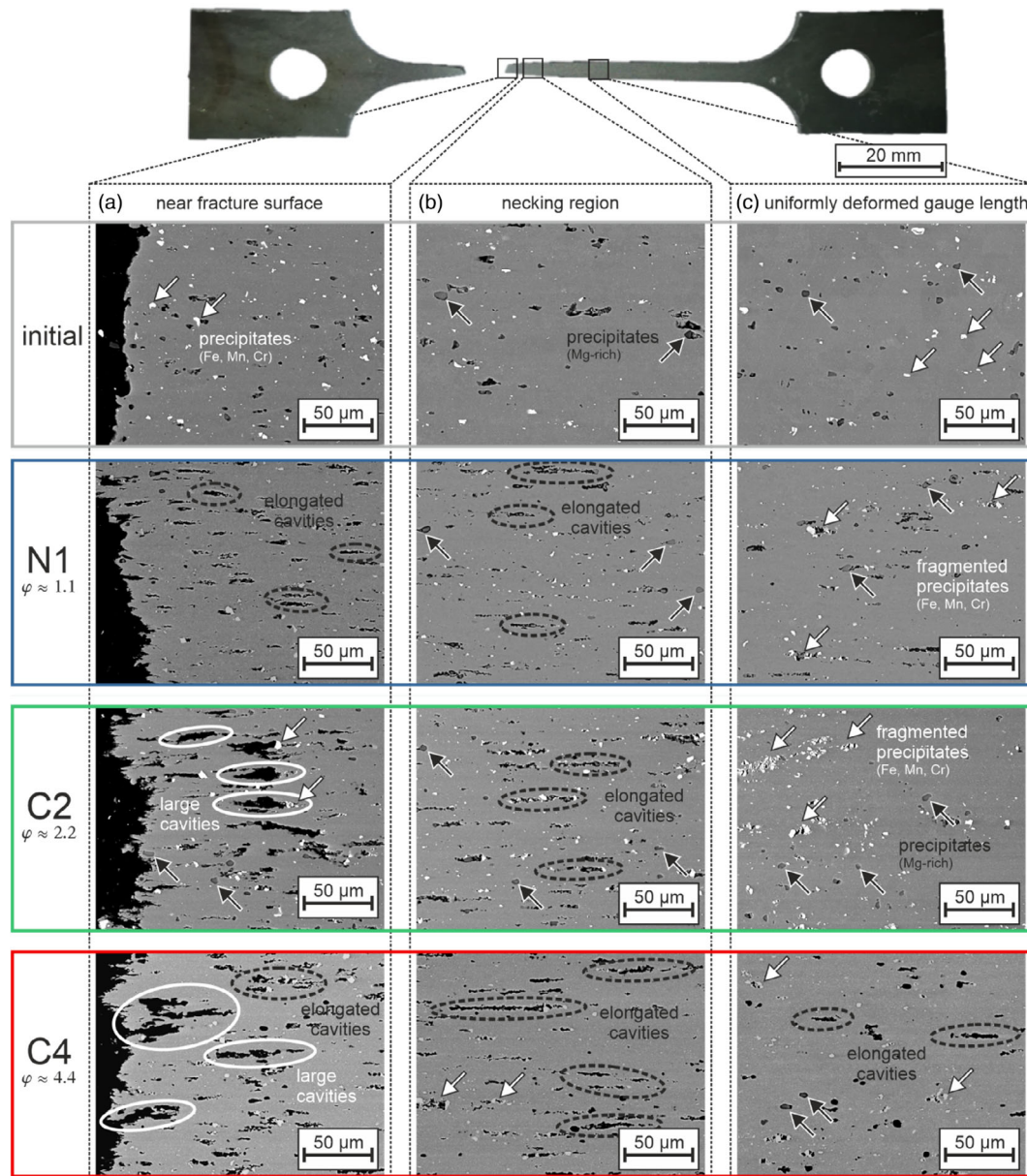


Figure 10. SEM micrographs recorded in the x - z plane (see Figure 2) at different locations in tensile samples after testing at 250 °C: a) near the fracture surface, b) in the necking region, c) in the uniformly deformed gauge length. Different rows correspond to the different material conditions initial, N1, C2, and C4 (box colors are related to the corresponding microstructural and mechanical data, Figure 5, 7, and 8).

recorded from tensile specimens after testing at 250 °C, at three different locations (uniformly elongated gauge length; necking region; near the fracture surface). It should be noted that the microstructural images in Figure 10 correspond to significantly different equivalent plastic strains, which does not allow a direct conclusion about the deformation mechanisms involved. The microstructure contains two types of precipitates, which have sizes ranging from approximately 1 to 10 μm . The first type of precipitates, marked by white arrows, mainly contains Fe, Mn, and Cr and is characterized by an irregular, sharp-edged morphology. The second type of precipitates, marked by black arrows, is rich in Mg and exhibits a globular shape. While the

shapes of these precipitates remain almost unchanged during ECAP processing, fragmentation of the first type of precipitates occurs (see for example column (c) and similar observations on precipitate fragmentation in the study by Hockauf et al.^[40]).

It is often reported that the nucleation of cavities during plastic deformation results from stress concentrations at triple junctions or second-phase particles.^[41] As the cavities are formed at the interfaces between particles and the aluminum matrix, and as the fragmentation of the first type of precipitates creates further interfaces, these precipitates likely have a pronounced impact on cavity nucleation (column (c)). Careful observation reveals an increased number of cavities in the region of necking and near

the fracture surface while only a few cavities are found in the uniformly deformed gauge length (column (c)). It is furthermore obvious that the magnitude of deformation introduced by ECAP promotes a more extensive formation of cavities due to the larger local strains during subsequent tensile testing.

Finally, a particular arrangement of elongated cavities aligned parallel to the tensile axis is frequently observed, which can be understood as an elongated conjunction of expanding cavities.^[36] In the region of necking (column (b)), the formation of a few elongated cavities (marked by black dashed ellipses) with a length of up to 100 μm can be observed. In case of the fine-grained conditions (C2, C4) very large cavities (marked by white ellipses) are found near the fracture surface (column (a)). These cavities emerge from the coalescence of elongated cavities as a consequence of multiaxial stresses and large local strains. The increasing number of very large cavities is also an essential characteristic of the fracture surface, which most likely leads to the decrease in tensile strength at 250 °C in the fine-grained microstructures. While there is no doubt that thermally activated processes contribute to the elongation in the ECAP-deformed conditions, an accurate quantification of the involved processes requires additional in-depth experimental research.

4. Conclusion

Severe plastic deformation (SPD) of thin sheets by ECAP using a modified experimental method with different stack orientations was investigated. It was found that a specific stack orientation (B), with shearing in the RD–TD plane, and the use of supporting bulk materials located at both sides of the stacked sheets enables successful processing. The supporting bulk material has an increased height compared with the stacked sheets and is deformed first during processing, which helps to close the gap that is needed for inserting the stack of sheets into the channel. It furthermore ensures that the elastic expansion of the die during processing can be compensated. This approach prevents the sheets from buckling during ECAP, which is a key attribute that facilitates further processing (such as additional ECAP passes) of the SPD-processed sheet metals.

AA5083 sheets were deformed in single (N1) and multiple ECAP passes following route C (C2, C4) and were subsequently characterized in terms of their microstructures and mechanical properties. A pronounced grain refinement and an increased strength were observed for the ECAP-processed sheets, which is in line with similar results for ECAP-processed bulk materials. The ECAP-deformed conditions are still precursors to UFG materials as a high fraction of the boundaries is of low-angle type. These results highlight the potential of the stacked sheets approach for producing UFG sheet materials with a potential for superplastic deformation, and for a microstructural investigation of the related deformation mechanisms.

A first characterization of the deformation behavior at elevated temperatures of the produced fine-grained sheets was carried out. As superplasticity is promoted by increased temperatures, but the need to avoid dynamic recrystallization and grain growth creates an upper bound, DSC measurements were used to determine a suitable temperature (250 °C) for further investigations. Tensile tests at this temperature showed an

increasing elongation of the material, accompanied by a reduction of strength, with an increasing number of ECAP passes. Compared with the initial material condition a doubling of the elongation to failure (engineering stress–strain) was observed for the material deformed by multiple ECAP passes (C2, C4). This is in good agreement with the microstructural results that are characteristic for this number of ECAP passes. A subsequent SEM analysis of microstructural features at three different locations in the tensile specimens (uniformly elongated gauge length, necking region, and fracture surface region) revealed the presence of cavities. Considering the mechanical behavior at elevated temperatures, the overall results indicate the contribution of characteristic diffusion-controlled deformation mechanisms in the ECAP-deformed AA5083 sheets.

Acknowledgements

The authors gratefully acknowledge the German Research Foundation (Deutsche Forschungsgemeinschaft, DFG) for supporting this work carried out within the framework of the collaborative research projects VO 1487/32-1 and WA 2602/13-1. The authors thank Felix Schubert, Tom Petschowsky, Paul Seidel, and Marcus Böhme for supporting the tensile testing, the ECAP experiments, metallographic preparation, and EBSD measurements.

Open access funding enabled and organized by Projekt DEAL.

Conflict of Interest

The authors declare no conflict of interest.

Data Availability Statement

Research data are not shared.

Keywords

equal-channel angular pressing, severe plastic deformation, stacked sheets, superplasticity, ultrafine-grained

Received: February 26, 2021

Revised: April 14, 2021

Published online:

-
- [1] R. Z. Valiev, T. G. Langdon, *Prog. Mater. Sci.* **2006**, *51*, 881.
 - [2] V. M. Segal, *Metals* **2020**, *10*, 244.
 - [3] V. M. Segal, V. I. Reznikov, A. E. Dobryshevshiy, V. I. Kopylov, *Russ. Metall.* **1981**, *1*, 99.
 - [4] S. Frint, M. Hockauf, P. Frint, M. F. X. Wagner, *Mater. Des.* **2016**, *97*, 502.
 - [5] Z. Horita, T. Fujinami, T. G. Langdon, *Mater. Sci. Eng., A* **2001**, *318*, 34.
 - [6] T. C. Lowe, *JOM* **2006**, *58*, 28.
 - [7] R. Z. Valiev, I. P. Semenova, V. V. Latysh, A. V. Shcherbakov, E. B. Yakushina, *Nanotechnol. Russ.* **2008**, *3*, 593.
 - [8] D. Yamaguchi, Z. Horita, M. Nemoto, T. G. Langdon, *Scr. Mater.* **1999**, *41*, 791.
 - [9] S. Y. Chang, B. Du Ahn, S. K. Hong, S. Kamado, Y. Kojima, D. H. Shin, *J. Alloys Compd.* **2005**, *386*, 197.
 - [10] R. Y. Lapovok, *J. Mater. Sci.* **2005**, *40*, 341.
 - [11] P. Frint, M. F. X. Wagner, S. Weber, S. Seipp, S. Frint, T. Lampeke, *J. Mater. Process. Technol.* **2017**, *239*, 222.

- [12] S. H. H. Najafabadi, A. A. L. Neyestanak, S. Daneshmand, *Ind. Lubr. Tribol.* **2017**, 69, 701.
- [13] Y. Iwahashi, M. Furukawa, Z. Horita, M. Nemoto, T. G. Langdon, *Metall. Mater. Trans. A. Phys. Metall. Mater. Sci.* **1998**, 29, 2245.
- [14] R. E. Barber, T. Dudo, P. B. Yasskin, K. T. Hartwig, *Scr. Mater.* **2004**, 51, 373.
- [15] M. Kamachi, T. Fujinami, Z. Horita, T. G. Langdon, *Mater. Sci. Forum* **2004**, 447–448, 477.
- [16] M. Lewandowska, W. Chrominski, M. Lipinska, L. Olejnik, A. Rosochowski, *Key Eng. Mater.* **2016**, 710, 59.
- [17] J. C. Lee, H. K. Seok, J. Y. Suh, *Acta Mater.* **2002**, 50, 4005.
- [18] J. Suh, J. Victoria-Hernandez, D. Letzig, R. Golle, S. Yi, J. Bohlen, W. Volk, *J. Mater. Process. Technol.* **2015**, 217, 286.
- [19] S. Seipp, M. F. X. Wagner, K. Hockauf, I. Schneider, L. W. Meyer, M. Hockauf, *Int. J. Plast.* **2012**, 35, 155.
- [20] M. F. X. Wagner, N. Nostitz, S. Frint, P. Frint, J. Ihlemann, *Int. J. Plast.* **2020**, 134, 102755.
- [21] P. F. Thomson, W. Song, *Int. J. Adv. Manuf. Technol.* **2018**, 96, 3691.
- [22] M. Mahmoodi, M. Sedighi, D. A. Tanner, *Mater. Des.* **2012**, 40, 516.
- [23] Y. Estrin, K. H. Rhee, R. Lapovok, P. F. Thomson, *J. Eng. Mater. Technol. Trans. ASME* **2007**, 129, 380.
- [24] R. Lachhab, M. A. Rekik, H. Azzeddine, T. Baudin, A. L. Helbert, F. Brisset, M. Khitouni, *J. Mater. Sci.* **2019**, 54, 4354.
- [25] P. Frint, M. Hockauf, T. Halle, M. F. X. Wagner, T. Lampke, *Materwiss. Werksttech.* **2012**, 43, 668.
- [26] M. Kamachi, M. Furukawa, Z. Horita, T. G. Langdon, *Mater. Sci. Eng., A* **2003**, 361, 258.
- [27] Y. Iwahashi, J. Wang, Z. Horita, M. Nemoto, T. G. Langdon, *Scr. Mater.* **1996**, 35, 143.
- [28] I. L. Dillamore, W. T. Roberts, *Acta Metall.* **1964**, 12, 281.
- [29] P. Frint, M. F. X. Wagner, *Acta Mater.* **2019**, 176, 306.
- [30] I. J. Beyerlein, C. N. Tomé, *Mater. Sci. Eng., A* **2004**, 380, 171.
- [31] S. P. Joshi, C. Eberl, B. Cao, K. T. Ramesh, K. J. Hemker, *Exp. Mech.* **2009**, 49, 207.
- [32] A. Benallal, T. Berstad, T. Børvik, O. S. Hopperstad, I. Koutiri, R. N. de Codes, *Int. J. Plast.* **2008**, 24, 1916.
- [33] M. Härtel, C. Illgen, P. Frint, M. F. X. Wagner, *Metals (Basel)*. **2018**, 8.
- [34] T. G. Langdon, *J. Mater. Sci.* **2009**, 44, 5998.
- [35] I. C. Hsiao, J. C. Huang, *Metall. Mater. Trans. A. Phys. Metall. Mater. Sci.* **2002**, 33, 1373.
- [36] K. T. Park, D. Y. Hwang, S. Y. Chang, D. H. Shin, *Metall. Mater. Trans. A. Phys. Metall. Mater. Sci.* **2002**, 33, 2859.
- [37] L. Dupuy, J. J. Blandin, *Acta Mater.* **2002**, 50, 3253.
- [38] H. W. Höppel, M. Prell, L. May, M. Göken, *Procedia Eng.* **2010**, 2, 1025.
- [39] L. H. Su, C. Lu, L. Z. He, L. C. Zhang, P. Guagliardo, A. K. Tieu, *Acta Mater.* **2012**, 60, 4218.
- [40] M. Hockauf, L. W. Meyer, D. Nickel, G. Alisch, T. Lampke, B. Wielage, L. Krüger, *J. Mater. Sci.* **2008**, 43, 7409.
- [41] R. Raj, M. F. Ashby, *Acta Metall.* **1975**, 23, 653.